

Color sensitive response of graphene / graphene quantum dot phototransistors

Paolo Fantuzzi^{1,2}, Andrea Candini^{2,3}, Qiang Chen⁴, Xuelin Yao⁴, Tim Dumsclaff⁴, Neeraj Mishra⁵, Camilla Coletti^{5,6}, Klaus Müllen^{4,7}, Akimitsu Narita^{4,8}, M. Affronte^{1,2**}*

¹Dipartimento di Scienze Fisiche, Matematiche e Informatiche, Università di Modena e Reggio Emilia, via G. Campi 213/A, 41125/A Modena. Italy

²Centro S3, Istituto Nanoscienze - CNR, via G. Campi 213/A, 41125 Modena. Italy

³Istituto per la Sintesi Organica e Fotoreattività ISOF - CNR, via Gobetti 101, 40129 Bologna

⁴Max Planck Institute for Polymer Research, Ackermannweg 10, D-55128 Mainz, Germany.

⁵Center for Nanotechnology Innovation @ NEST, Istituto Italiano di Tecnologia, Piazza San Silvestro 12, 56127 Pisa, Italy

⁶Graphene Labs, Istituto Italiano di Tecnologia, via Morego 30, 16163 Genova, Italy

⁷Institute of Physical Chemistry, Johannes Gutenberg University Mainz, Duesbergweg 10-14, D-55128 Mainz, Germany

⁸Organic and Carbon Nanomaterials Unit, Okinawa Institute of Science and Technology Graduate University, Okinawa 904-0495, Japan

ABSTRACT

We present the fabrication and characterization of all-carbon phototransistors made of graphene three terminal devices coated with atomically precise graphene quantum dots (GQD). Chemically synthesized GQDs are the light absorbing materials, while the underlying chemical vapor deposition (CVD)-grown graphene layer acts as the charge transporting channel. We investigated three types of GQDs with different sizes and edge structures, having distinct and characteristic optical absorption in the UV-Vis range. The photoresponsivity exceeds 10^6 A/W for vanishingly small incident power ($<10^{-12}$ W), comparing well with state of the art sensitized graphene photodetectors. More importantly, the photoresponse is determined by the specific absorption spectrum of each GQD, exhibiting the maximal responsivity at the wavelengths corresponding to the absorption maxima. Overall this behavior can be ascribed to the efficient and selective absorption of light by the GQDs, followed by a charge transfer to graphene, a mechanism known as photogating effect. Our results suggest the use of graphene/GQD devices as valuable photodetectors for application where color sensitivity is required.

1. INTRODUCTION

The high carrier mobility of graphene is an appealing characteristic for the realization of optoelectronic converters¹, since it ensures that the charges created by the light rapidly reach the electrodes, thus minimizing the recombination effect and efficiently converting the incoming photons into an electric signal. Furthermore, since graphene is a material with zero band gap, charges can be generated by the absorption of light over a wide energy spectrum, from the short-wavelength terahertz to the more energetic photons in the UV range². However, the direct use of pristine graphene is limited due to its atomic thickness and hence transparency. Several ways to improve the absorption of electromagnetic radiation of graphene have been proposed and tested³. A convenient approach to achieve photon detection even at very low intensity is to combine conductive graphene with photo-active sensitizing systems, such as colloidal nanocrystals⁴, nanoparticles⁵ and other two dimensional materials such as MoS₂⁶, that absorb light very efficiently. Following the photon absorption, either electrons or holes are transferred to graphene, while the other type of charge remain trapped into the photo-active center, thus working as an effective local electrostatic gate for the graphene sheet, where charges are recirculated many times from source to drain. This mechanism is known as photo-gating effect⁷ and it is characterized by high gain (i.e. multiple electrical carriers are detected per incident photon), thus leading to high sensitivity. In these previous works the light absorption spectra are usually broad and feature a threshold, which depends on the size of the nanocrystals and nanoparticles on top of graphene or on the magnitude of the energy band gap in the case of MoS₂ layers.

In this context, the possibility to realize color-sensitive photodetectors, that is devices that respond to a specific wavelength only, would be extremely valuable and it has been actually proposed for a wide set of applications including sensing and energy harvesting, where the energy

selectivity can be exploited as an additional functionality or for the optimization of the efficiency, or as component in neural / bio -inspired networks^{8,9}. Color sensitive devices have been realized by enhancing the light absorption by plasmonic effects¹⁰ or by making use of photo-chromic molecules that undergo reversible photo triggered isomerization between metastable states¹¹.

Ideally, color detection and high sensitivity can be combined by functionalizing graphene with light-absorbing molecules with a well-defined and narrow absorption spectrum. An intriguing possibility is to use graphene quantum dots (GQDs), which are nanoscale fragments of graphene, with non-zero energy gaps due to the quantum confinement effect¹²⁻¹⁴. Depending on the sizes and structures of the graphene fragments, they absorb and emit light at different wavelengths and are therefore attracting increasing attentions for applications in opto-electronic devices¹⁵⁻¹⁷. In addition, they are also metal-free, low-cost and environment-friendly. However, previous attempts to realize graphene/GQD photodetectors made use of undefined GQDs, without a precise control over their chemical structures, such as shapes and edge configurations. This resulted in broad absorption spectra, unsuitable for color-selective optical sensors¹⁸. Bottom-up chemical synthesis provides access to atomically precise GQDs, which are also called nanographenes or graphene molecules¹⁹⁻²⁰. Various atomically precise GQDs have thus been synthesized, demonstrating structure-specific opto-electronic properties, with well-defined optical absorption spectra²¹⁻²⁴. Although pristine, hydrogen-terminated GQDs are insoluble due to the strong π - π stacking interactions, it is possible to install solubilizing alkyl chains at the edges through proper synthetic designs²⁵, without altering the optical properties that remain determined mostly by the aromatic core structure²⁶. Such precisely designed and bottom-up-synthesized GQDs can thus be soluble in organic solvents and processed from solutions, allowing for facile integration into opto-electronic devices.

Here we use atomically precise GQDs with three different chemical structures and optical properties as selective light absorbing material to realize all-carbon phototransistors, showing both color-selectivity and high photoresponsivity. The easy deposition from solution and the tunability of the GQD absorption properties make them suitable for sensitive photodetectors based on graphene (or other two-dimensional materials) when color-sensitive applications are required²⁷⁻²⁹.

2. EXPERIMENTAL SECTION

2.1. Preparation of graphene quantum dots. We selected three different atomically precise GQDs for this study, namely **C60-8-C12** consisting of 60 sp² carbon atoms in the aromatic core that is functionalized with eight *n*-dodecyl (C₁₂H₂₅) chains³⁰, 6,14-bis{3,4,5-tris(dodecyloxy)phenyl}dibenzo[*hi,st*]ovalene (**DBOV-TDOP**)³¹, and “tetra-zigzag” hexa-*peri*-hexabenzocoronene (**TZHBC**)³², whose chemical structures are shown in Figure 1a. These three GQDs were bottom-up synthesized using techniques of synthetic organic chemistry, as described in our previous reports³⁰⁻³². The peripheral functionalization groups are added to increase the dispersibility of the molecules in organic solvent, while their effects on the optical properties remain negligible^{26,30-32}. UV-VIS absorption spectra of the three GQDs in solution displayed distinct profiles with onsets at ~580, ~640, and ~700 nm for **C60-8-C12**, **DBOV-TDOP**, and **TZHBC**, respectively (Figure 1b).

2.2. Device fabrication and characterization. We used large-area monolayer graphene produced by chemical vapor deposition (CVD) and transferred on a chip of p⁺⁺ bulk Si, covered by 300 nm of SiO₂, which is used as the common backgate, following a reported procedure³³. Devices were fabricated through Electron Beam Lithography to etch the graphene sheet and pattern

the gold pads for electrical contacts. The GQDs, namely **C60-8-C12**, **DBOV-TDOP**, and **TZHBC**, were deposited on the device by drop casting. The procedure of deposition was done as follows: 5 mg of GQD powder was dispersed in 100 mL of dichloromethane and sonicated until the dispersion had an uniform color without any visible aggregate. 100-200 μL of the dispersion was then deposited on the devices by using a micropipette. In order to accelerate the evaporation of the solvent, the chip has been kept on a hot plate at 75°C during the deposition. In the following we use the same code as for the GQDs (that is **C60-8-C12**, **DBOV-TDOP**, **TZHBC**) to label the corresponding devices.

The structural characterization has been done with optical microscope and Scanning Electron Microscope (SEM), while (photo-)electrical characterizations were done by using Lake Shore probe station at room temperature and in vacuum (pressure of 10^{-4} mbar). The source-drain voltage V_{ds} , the backgate voltage V_{g} and the measurements of the current I_{ds} of the graphene devices were carried out by a Keithley 2636B double channel source-meter. The devices were illuminated with a white light lamp placed directly on top of the probe station. Alternatively, for the wavelength selective investigations, we either placed a monochromator in front of the lamp or employed two lasers with wavelengths 638 and 374 nm, respectively. The corresponding illumination power was estimated with a calibrated photodiode placed at the sample position.

3. RESULTS AND DISCUSSIONS

3.1. Electrical and opto-electrical characterization. Figure 1c shows our typical devices. Thanks to the large area of CVD-grown graphene, on a single chip it was possible to fabricate c.a. 100 junctions per chip. The final substrate was cut into more parts in order to make different GQD depositions. The results shown here are representative of the observed general behavior.

Figure 1d displays typical transfer characteristics I_{ds} vs V_g of the pristine graphene (black curve) along with those taken after the deposition of **TZHBC** with (red curve) and without (blue curve) light illumination. Note that the neutrality point is not visible in the gate voltage range of ± 60 V suggesting large p-doping of our pristine graphene layer. For pristine graphene the light does not affect the transfer characteristic, thus confirming the low efficiency of light-charge conversion of pristine graphene as largely reported in literature^{2,3}. The mobility μ of our pristine conducting layer can be estimated through the expression for field-effect-transistors in the linear region^{34,35}:

$$\mu = [dI_{ds}/dV_g] \cdot [L/(D C_i V_{ds})]$$

where dI_{ds}/dV_g is extracted from a linear fit of the transfer characteristics; L and D are, respectively, the length and the width of the conductive channel of our device; C_i is the gate capacitance and V_{ds} the applied drain-source voltage. Taking $L = 4 \mu\text{m}$ (the distance between source and drain) and $D = 10 \mu\text{m}$, (the width of the graphene sheet), we can estimate $\mu \sim 400 \text{ cm}^2/\text{V}\cdot\text{s}$. After the deposition of the molecules, the mobility μ decreases to values ranging from 170 to 130 $\text{cm}^2/\text{V}\cdot\text{s}$. The mobility reduction after the deposition has been observed also in similar devices⁵ and can be related to the additional disorder induced by the GQDs. Upon illumination (white light with intensity of 24.7 mW/cm^2) we observe that the I_{ds} vs V_g curve is rigidly shifted towards higher backgate values, corresponding to a significant current increase larger than 20% and a similar mobility.

3.2. Photoresponse. Figure 2a shows typical current photoresponse of our devices. Here V_{ds} and V_g are constant at 100 mV and +40 V respectively, while the light wavelength is 561 nm. After an initial delay needed to stabilize the response, light is repeatedly turned *on* and *off* (green dashed line in Figure 2a). The inset in Figure 2a zooms on the *on/off* switches of the light. The time scale

of minutes evidences a slow photoresponse, as it is found in sensitized graphene photodetectors characterized by a disordered interface^{36,37} and other composite materials³⁸. From *off* to *on*-state, after a rapid increase, the current reaches the full saturation value in a timescale of minutes; from *on* to *off* the process is even slower and the current typically recovers the initial value (before the light pulse) in tens of minutes. Over long (hour) time scales, the observed behavior is stable and the light can be turned *on-off* for an indefinite number of times with no evident signs of degradation of the electrical signal or the optical response.

Figure 2b exhibits the photoresponsivity R of the different GQDs-based phototransistors as a function of the illumination power (P). R is defined as the photocurrent (evaluated by taking the difference of I_{ds} when the light is *on* and *off*) divided by P . The sensitive surface of the device was estimated considering the active area of the channel with L and D as the lateral dimensions as introduced before. For illumination power ranging between 10^{-8} to 10^{-10} W, the measurements are done with white light, while for $P = 10^{-12}$ to 10^{-13} W measurements are done with monochromatic light, with the wavelength set at the corresponding maximum in the absorption spectra of each GQDs (see Figure 1b). We observe that for incident powers lower than 2×10^{-13} W, the **TZHBC** device exhibits a responsivity $R \sim 2.5 \times 10^7$ AW⁻¹ (measured with $V_{ds} = 100$ mV and $V_g = +40$ V). Such value gives a Noise Equivalent Power (NEP) $\sim 10^{-14}$ W, assuming the current noise as $\sim 10^{-7}$ A for an integration time of 1 s (Figure 2a). We notice that performances of our devices are of the same order of magnitude of values reported in literature for hybrid devices using nanocrystals⁴, nanoparticles⁵ or MoS₂⁶. Moreover, the power dependence of the photo-responsivity follows a similar phenomenological scaling law $f(P) = c1/(c2 + P)$, where $c1$ and $c2$ are the fitting parameters ($c2$ corresponds to a saturation value) and P is the illumination power^{4,5}.

Figure 3 displays the photoresponsivity as a function of the wavelength of the incident light for the three different GQDs, taken with $V_{ds} = 100$ mV, $V_g = 0$ V and power $P \sim 10^{-12}$ W. Within the accuracy of our monochromator (we estimate ± 20 nm the spread of the wavelengths around the central line), we observe that the photoresponsivity is related to the absorption spectrum of each GQD deposited on the graphene channel. For a direct comparison, the spectra (the same reported in Figure 1b) are also shown as continuous lines in the figure. **C60-8-C12** and **TZHBC** exhibit an enhancement of the photoresponsivity around 450 nm where they actually present a peak in their optical absorption spectra, along with additional structures centered at 500 nm and 600 nm for **C60-8-C12** and **TZHBC**, respectively. **DBOV-TDOP** shows a maximum in the absorption spectrum at 625 nm when measured in solution, while the measured photoresponsivity of the corresponding device exhibits a maximum at a shorter wavelength (~ 550 nm). This is probably due to the aggregation of the GQDs on top of the graphene sheet. Indeed, the absorption spectrum of **DBOV-TDOP** in a thick film (red line in Figure 3b) exhibits broader and blue shifted peaks with respect to the spectrum measured in solution (blue line).

In Figure 3c we also show measurement taken at different gate voltages ($V_g = -40$ V, 0 V, +40 V), observing that the photoresponse tends to be slightly higher for positive gate voltages, but the effect is very weak and within our experimental accuracy. This behavior, reported here for the case of the **TZHBC** molecule, is general and does not depend on the specific GQD used. The finding of a weak gate dependence of the photocurrent apparently differs from previously reported results on other sensitized graphene photodetectors, where the photoresponse is fully tuned by the gate voltage.^{4,5} We ascribe our observation to the large p-doping of our graphene sheet itself, as evidenced in Figure 1d. In the whole range of backgate voltage values, the devices are always far from the neutrality point and the I_{ds} vs V_g dependence is linear. Upon illumination, the transfer

characteristics are rigidly shifted towards more positive backgate values: as a consequence, the photocurrent values and hence the photodetector properties are only weakly dependent from the backgate voltage.

3.3. Time dependence of the photoresponse. We now discuss in more details the time dependence of the photoresponse. Figure 4 shows the profile of the current upon switching *on* / *off* the (white) light (power $\sim 10^{-9}$ W) for the case of the **DBOV-TDOP** compound (the other molecules show qualitatively similar results), where it is evident that the time evolution of the photocurrent is different when the light is turned *on* or *off*. Turning the light *on*, the photocurrent reaches 65% of the saturation value in ~ 2 s then it increases more slowly eventually reaching saturation. This observation suggests that two mechanisms with different time scales take place and we consider a double exponential function to fit the I_{ds} vs time curves:

$$y(t) = y_0 + A_1 \cdot e^{-(t-t_0)/\tau_1} + A_2 \cdot e^{-(t-t_0)/\tau_2}$$

When the light is switched *off*, the current comes back to the initial value in a time scale of tens of minutes. In this case a stretched exponential of the type:

$$y(t) = I_0 + A \cdot e^{-(t/\tau)^\beta}$$

better fits the experimental data, suggesting that this relaxation process takes place in a disordered system, likely with the contribution of different mechanisms.

3.4. Mechanism of the photoresponse. Based on the previous observations, we sketch in Figure 5 the functioning model of our devices, that qualitatively accounts for the reported behavior, in agreement with related works reported in the literature³. We expect that the charge current preferentially flows in the graphene channel which has higher mobility with respect to the GQD

layer. Since the pristine graphene is p-doped (see Figure 1d), the carriers forming the current I_1 are thus represented as holes in Figure 5a (up panel). When the light is turned *on* (Figure 5a, bottom panel), photons are absorbed by the GQDs, with an efficiency that is related to the characteristic absorption spectrum of each GQD, creating electron-hole pairs. These may induce two effects on the graphene channel:

- 1) The GQDs which are in contact with the graphene layer transfer the holes to the conductive graphene sheet, inducing an increase of the free carrier density and therefore of $I_2 > I_1$.
- 2) The photo-induced electrons remain trapped in the GQDs, creating a local electric field. In practice, they act as a second gate voltage near the flowing carriers (*photogating effect*³).

A simple estimation of the first effect indicates that it is almost negligible for the measured photocurrent. Indeed, for an incident light intensity equal to 1 mW/cm² and a photon energy 3.2×10^{-19} J (c.a. 2 eV, ~600 nm), the resulting photons flux Φ on the GQDs is:

$$1 \text{ mW/cm}^2 = 1 \times 10^{-3} \text{ J/s} \cdot \text{cm}^2 = 1 \times 10^{-3} / 3.2 \times 10^{-19} \text{ photons/s} \cdot \text{cm}^2 \approx 3 \times 10^{16} \text{ photons/s} \cdot \text{cm}^2$$

Since the area of our devices is of the order of tens of μm^2 , the flux of photons on the device is from 10^9 to 10^{10} photons/s. Even if we assume a perfect efficiency (i.e. each photon is converted in one electron), this flux would correspond to a photocurrent of nA (multiplying the flux by the electron charge). This value of current is far below the lowest photocurrent that we measured (c.a. 1 μA). This implies that the number of holes injected in the graphene layer are negligible for the determination of the photocurrent. Conversely, the photogating effect usually leads to a significant *gain* $\gg 1$, since the electrons remains trapped in the GQDs for a time τ_{lifetime} that is long compared to the time needed by the holes to transit through the device. This timescale is defined as τ_{transit} and it is proportional to $\sim L^2 / \mu V_{\text{ds}}$, where L is the distance between electrodes, μ is the charge mobility and V_{ds} is the applied source-drain bias. Indeed, the photogating *gain* G_{ph} is usually defined as the

ratio between this two timescales: $\tau_{\text{lifetime}} / \tau_{\text{transit}}$. To assess the consistency of this simple model we relate the measured responsivity R with the estimated gain G_{ph} . At a given power: $R = G_{\text{ph}} \times \text{QE} \times q/h\nu$, where q is the electron charge, $h\nu$ the photon energy and QE is the external quantum efficiency accounting for both the light absorption efficiency and the charge transfer efficiency. Under our experimental conditions, QE can be evaluated by a simple parallel plate capacitor model⁵. Referring to the results shown in Figure 1d, we observe that a light power of $\sim 10^{-9}$ W, corresponding to a flux $\sim 10^{18}$ photons/s·cm², induces a positive shift of the device transfer curve of ~ 50 V. Since the backgate capacitive coupling is 7×10^{10} cm⁻²V⁻¹ this implies that, during 1 s, a negative charge density of $\sim 10^{12}$ cm⁻² is accumulated on the GQD. At this power, the efficiency of our device is thus 10^{-6} . To calculate the gain $G_{\text{ph}} = \tau_{\text{lifetime}} / \tau_{\text{transit}}$, we consider $L = 4$ μm , $\mu = 200$ cm²/Vs, $V_{\text{ds}} = 0.1$ V yielding $\tau_{\text{transit}} \sim 10^{-8}$ s; the lifetime of the photoexcited trapped states on the GQD can be evinced by the data of Figure 3c (still performed with a light power of $\sim 10^{-9}$ W), giving $\tau_{\text{lifetime}} \sim 10^2$ s. This leads to $G_{\text{ph}} \sim 10^{10}$ and $R \sim 10^4$ A/W for a photon wavelength ~ 600 nm, that is in agreement with the measured value at the light power which we considered for this case.

In Figure 5b we report the photoconductive mechanism from the point of view of the energy levels. The scheme is corroborated also by the published values of the GQD highest occupied molecular orbital (HOMO) energy levels, as calculated by density functional theory, from which we can estimate the GQD work function to be $> \sim 5$ eV^{32,39}, that is higher than the graphene work function, also when it is heavily p-doped⁴⁰, as in our case. As the absorbed photons create electron-hole pairs, the electrons remains trapped on an excited energy level of the GQDs, while the holes are transferred to the graphene. The built-in electric field (electrons) and the transferred charges (holes) correspond to a photo-doped charge transport in the graphene sheet.

Finally, we summarize the properties of the different compounds in Table 1.

4. CONCLUSIONS

In summary, we realized all-carbon (graphene - graphene quantum dots) photodetectors made of a large scale CVD graphene and atomically defined graphene quantum dots. For low impinging radiation power ($< 10^{-12}$ W) the photoresponsivity attains 10^7 A/W. The corresponding detectivity D^* ($D^* = (A \times BW)^{0.5} / \text{NEP}$, where A is the device area, BW the bandwidth and NEP the noise equivalent power) is estimated as 6×10^9 Jones ($\text{cm Hz}^{1/2} \text{ W}^{-1}$), considering an area of $40 \mu\text{m}^2$ and a bandwidth of 10^{-2} Hz. With respect to the state of the art values⁵, our devices are limited mainly by the slow dynamic. We believe that the long time response can be largely reduced by increasing the quality of the conducting graphene sheet and by the optimization of the deposition of the GQDs (for instance by using the electro-spray⁴¹ technique). This will allow to tune efficiently the photoresponse with the backgate thus speeding up the response of the devices through the use of voltage pulses⁵.

The main point of our work is that the peculiar absorption spectra of each GQD is reflected in the spectral dependence of the device photoresponse. These characteristics can be exploited for different applications. For instance, the use of tailor made light-absorbing molecules can be considered for the optimization of energy harvesting performances of photo-current converters. Alternatively spectral selective responses can be used in light operational devices, such as bio-inspired (neuromorphic) circuits, where the sum of two or more laser signals are selectively converted to an electrical digital signal.

FIGURES

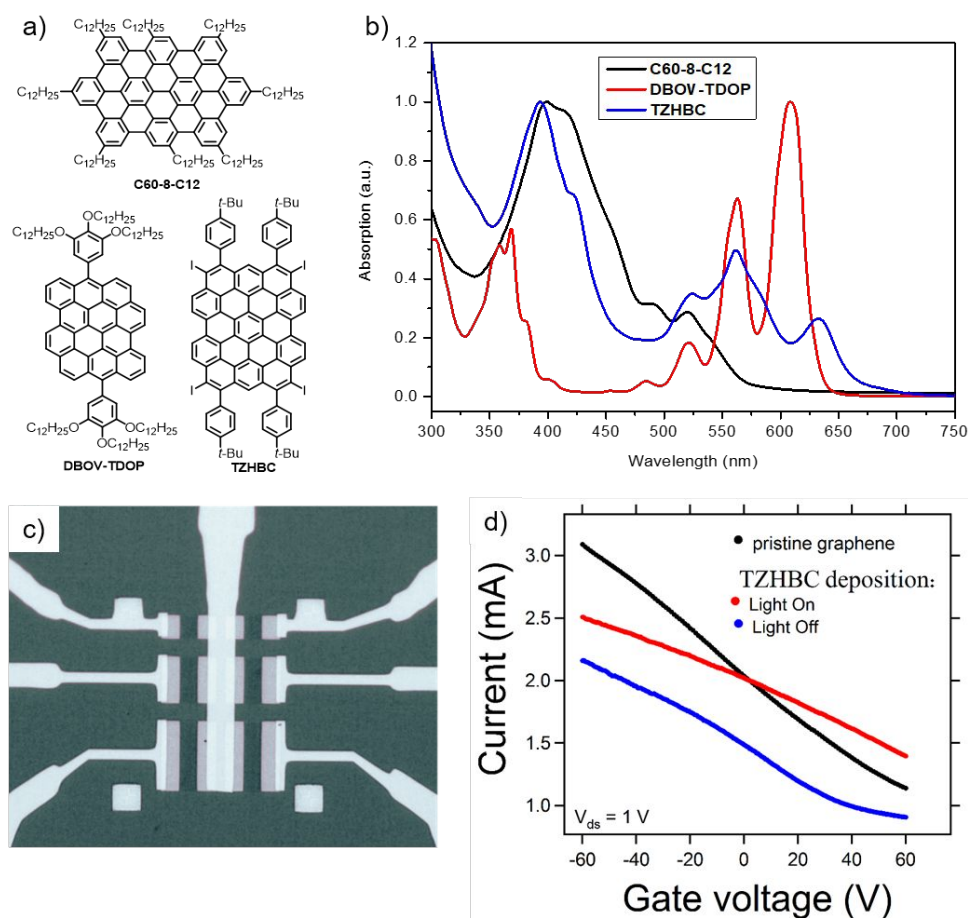


Figure 1. a) Chemical structures of three different GQDs and (b) their corresponding UV-VIS absorption spectra measured in toluene (**C60-8-C12** and **DBOV-TDOP**) and tetrahydrofuran (**TZhBC**) at a concentration of 10^{-5} M. The corresponding molar extinction (absorption) coefficients at their maximum absorption wavelength are $\sim 9.7 \times 10^4 \text{ M}^{-1}\text{cm}^{-1}$, $\sim 3.9 \times 10^5 \text{ M}^{-1}\text{cm}^{-1}$ and $\sim 2.0 \times 10^4 \text{ M}^{-1}\text{cm}^{-1}$, for the **C60-8-C12**, **DBOV-TDOP** and **TZhBC** compounds, respectively. c) Optical image of the graphene junctions. The horizontal size is $80 \mu\text{m}$. d) Comparison between the transfer characteristics before and after the deposition of **TZhBC**. (White light with intensity 24.7 mW/cm^2 , corresponding to a power $\sim 10^{-9} \text{ W}$).

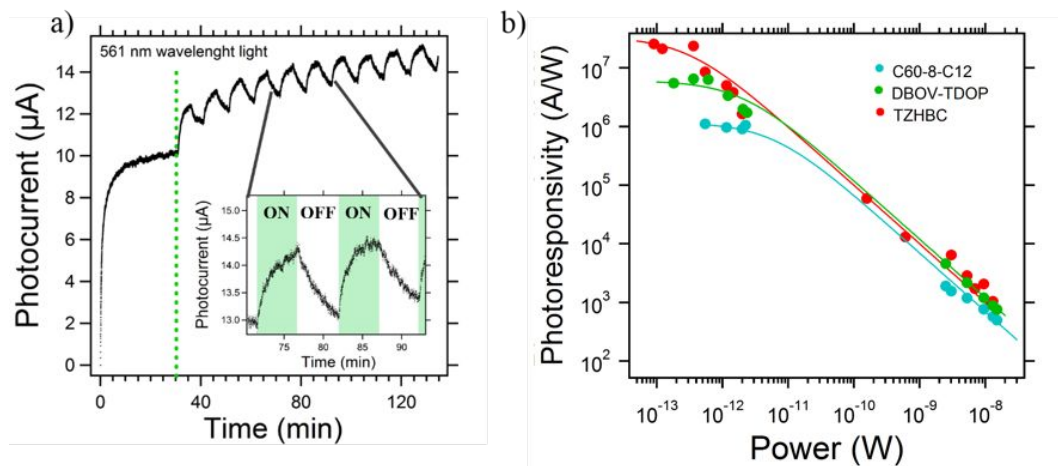


Figure 2: a) Typical time evolution of the photocurrent as measured on a **TZhBC** device, $V_{ds} = 100$ mV and $V_g = +40$ V. The inset shows a zoom in the region where the light is turned *on* and *off* repeatedly. Light at 561 nm ($3 \mu\text{W}/\text{cm}^2$) from the monochromator has been used in this case. b) Responsivity as a function of the illumination power. The solid lines are the best fit to the data using the typical phenomenological function used in literature^{4,5}: $f(P) = c1/(c2 + P)$, where $c1$ and $c2$ are free fitting parameters and P is the light power. Here $c1 = 7 \times 10^{-6}$ A; 12×10^{-6} A; 1×10^{-5} A; and $c2 = 6 \times 10^{-12}$ W; 2×10^{-12} W; 3×10^{-13} W for C60-8-C12; DBOV-TDOP; TZhBC, respectively.

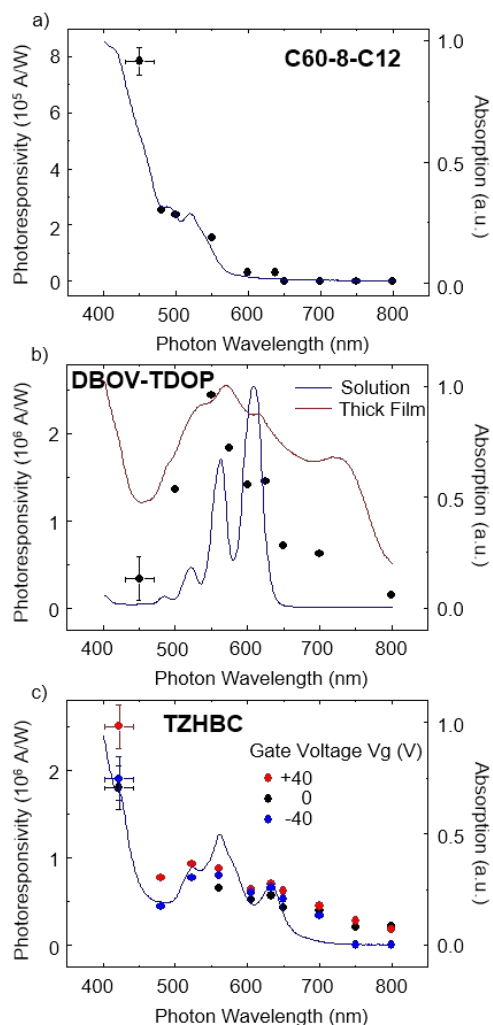


Figure 3. Photoresponsivity (dots, left Y-axis) of the G/GQD devices as a function of the incident light wavelength for **C60-8-C12** (a), **DBOV-TDOP** (b) and **TZhBC** (c). For comparison, also the corresponding absorption spectra taken on the molecule in solution (continuous lines, right Y-axis) are superimposed. Experimental conditions: $V_{ds} = 100$ mV; $V_g = 0$ V; power $P \sim 10^{-12}$ W. For the DBOV-TDOP molecule in b) also the absorption spectra of the thick film is shown (red line), evidencing a blue-shift and a broadening of the absorption maximum. For clarity, the error bars are showed only for the first data point of each set, but they are to be considered also for the other points (with the same size).

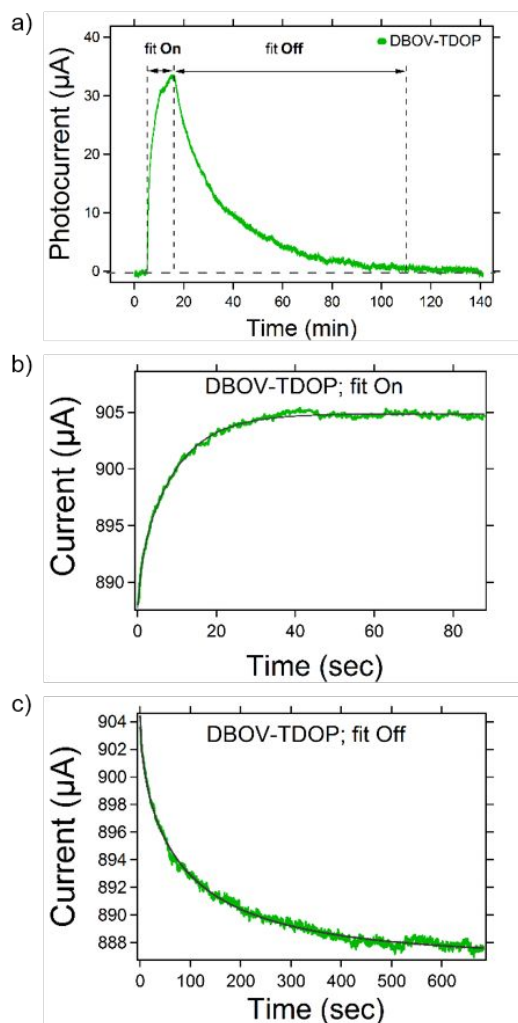


Figure 4. a) Photocurrent response of **DBOV-TDOP** device (white light with power $\sim 10^{-9}$ W). b)

The *on* light response is fit with a double exponential function of the type $y(t) \sim e^{(-t/\tau_1)} + e^{(-t/\tau_2)}$

, where $\tau_1 \sim 1$ s and $\tau_2 \sim 10$ s. c) When the light is turned *off* the photocurrent is fit with a

stretched exponential function $y(t) \sim e^{-(t/\tau)^\beta}$, where $\tau \sim 90$ s and $\beta \sim 0.6$.

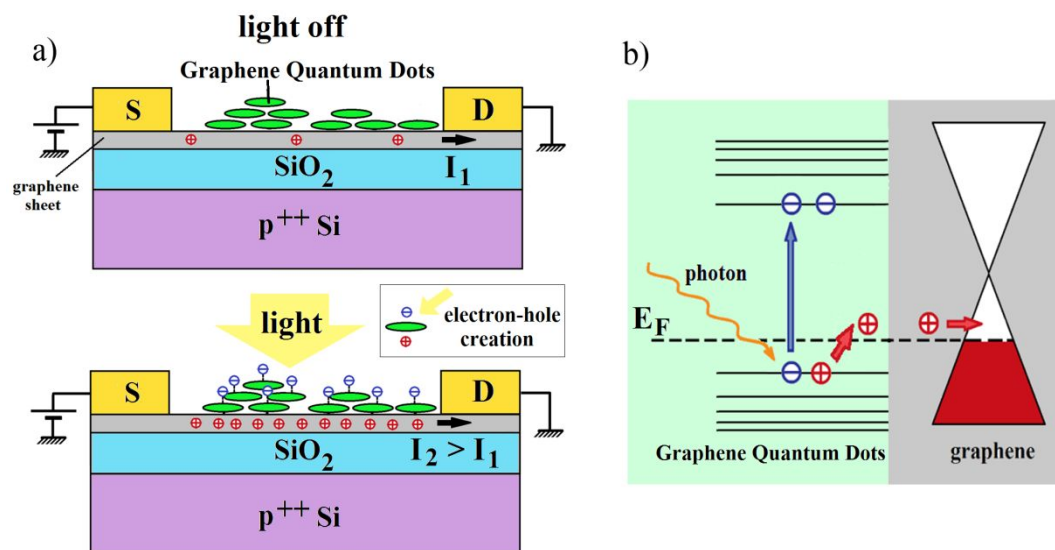


Figure 5. a) Functioning scheme of the device with the light *off* (up) and *on* (bottom). I_1 is the (hole) current of the device with no light excitation. I_2 is the enhanced current due to the photoexcitation. Electrons remain trapped in the GQDs, while holes are transferred to the graphene sheet. b) Corresponding scheme of the energy diagram, showing the photoexcitation mechanism.

Graphene Quantum Dot sensitizer	Wavelength for Absorption Maximum	Wavelength for Photoresponsivity Maximum	Photoresponsivity @ 10^{-13} W	Decay time τ
C60-8-C12	~ 400 nm	~ 400 nm	$\sim 10^6$ A/W	60 s
DBOV-TDOP	~ 600 nm	~ 550 nm	$\sim 5 \times 10^6$ A/W	90 s
TZHBC	~ 400 nm	~ 400 nm	$\sim 10^7$ A/W	300 s

Table1. Summary of the three GQD compounds used in this work. The wavelength corresponding to the absorption maximum has been measured for the molecule in solution, while that for the photoresponsivity maximum is the direct measurements of the device (Graphene functionalized with GQD) photoresponse. The decay time τ has been measured after turning off the light (power $\sim 10^{-9}$ W) following the same procedure described in Figure 4c.

AUTHOR INFORMATION

Corresponding Author

*andrea.candini@isof.cnr.it Phone: +39 051 6399853

**marco.affronte@unimore.it Phone: +39 059 2058375

Note

The authors declare no competing financial interest.

ACKNOWLEDGMENT

This work has been partially supported by the European Community through the FET-Proactive Project “MoQuaS” contract N.610449, by the Italian Ministry for Research (MIUR) through the Futuro In Ricerca (FIR) grant RBFR13YKWX. The research leading to these results has received funding from the European Union’s Horizon 2020 research and innovation program under grant agreements Nos. 696656 – GrapheneCore1 and 785219 – GrapheneCore2 and by the DFG Priority Program SPP 1459 and by the Office of Naval Research BRC Program.

REFERENCES

1. Novoselov, K. S.; Fal’ko, V. I.; Colombo, L.; Gellert, P. R.; Schwab, M. G.; Kim, K. A roadmap for graphene. *Nature* **2012**, *490*, 192-200.
2. Bonaccorso, F.; Sun, Z.; Hasan, T.; Ferrari, A. C. Graphene photonics and optoelectronics. *Nat. Photonics* **2010**, *4*, 611-622.
3. Koppens, F. H. L.; Mueller, T.; Avouris, P.; Ferrari, A. C.; Vitiello, M. S.; Polini, M. Photodetectors based on graphene, other two-dimensional materials and hybrid systems. *Nat. Nanotechnol.* **2014**, *9*, 780-793.
4. Spirito, D.; Kuder, S.; Miseikis, V.; Giansante, C.; Coletti, C.; Krahne, R. UV light detection from CdS nanocrystal sensitized graphene photodetectors at kHz frequencies. *J. Phys. Chem. C* **2015**, *119*, 23859-23864.
5. Konstantatos, G.; Badioli, M.; Gaudreau, L.; Osmond, J.; Bernechea, M.; Garcia de Arquer, F. P.; Gatti, F.; Koppens, F. H. L. Hybrid graphene–quantum dot phototransistors with ultrahigh gain. *Nat. Nanotechnol.* **2012**, *7*, 363-368.

6. Roy, K.; Padmanabhan, M.; Goswami, S.; Phanindra Sai, T.; Ramalingam, G.; Raghavan, S.; Ghosh, A. Graphene–MoS₂ hybrid structures for multifunctional photoresponsive memory devices. *Nat. Nanotechnol.* **2013**, *8*, 826-830.
7. Rowe, M. A.; Gansen, E. J.; Greene, M.; Hadfield, R. H.; Harvey, T. E.; Su, M. Y.; Nam, S. W.; Mirin, R. P. Single-photon detection using a quantum dot optically gated field-effect transistor with high internal quantum efficiency. *Appl. Phys. Lett.* **2006**, *89*, 253505.
8. Qin, M.; Huang, Y.; Li, F.; Song, Y. Photochromic sensors: a versatile approach for recognition and discrimination. *J. Mater. Chem. C* **2015**, *3*, 9265-9275.
9. Zhang, X.; Hou, L.; Samorì, P. Coupling carbon nanomaterials with photochromic molecules for the generation of optically responsive materials. *Nat. Commun.* **2016**, *7*, 11118.
10. Liu, Y.; Cheng, R.; Zhou, H.; Bai, J.; Liu, G.; Liu, L.; Huang, Y.; Duan, X. Plasmon resonance enhanced multicolour photodetection by graphene. *Nat. Commun.* **2011**, *2*, 579.
11. Zhou, X.; Zifer, T.; Wong, B. M.; Krafcik, K. L.; Léonard, F.; Vance, A. L. Color detection using chromophore-nanotube hybrid devices. *Nano Lett.* **2009**, *9*, 1028-1033.
12. Zheng, P.; Wu, N. Fluorescence and sensing applications of graphene oxide and graphene quantum dots: A Review. *Chem. – An Asian J.* **2013**, *12*, 2343-2353.
13. Li, X.; Rui, M.; Song, J.; Shen, Z.; Zeng, H. Carbon and graphene quantum dots for optoelectronic and energy devices: a review. *Adv. Func. Mater.* **2015**, *25*, 4929-4947.

14. Li, L.; Wu, G.; Yang, G.; Peng, J.; Zhao, J.; Zhu, J.-J. Focusing on luminescent graphene quantum dots: current status and future perspectives. *Nanoscale* **2013**, *5*, 4015.
15. Dinari, M.; Momeni, M.; Goudarzirad, M. Dye-sensitized solar cells based on nanocomposite of polyaniline/graphene quantum dots. *J. Mater. Sci.* **2016**, *51*, 2964-2971.
16. Mihalache, I.; Radoi, A.; Mihaila, M.; Munteanu, C.; Marin, A.; Danila, M.; Kusko, M.; Kusko, C. Charge and energy transfer interplay in hybrid sensitized solar cells mediated by graphene quantum dots. *Electrochim. Acta* **2015**, *153*, 306-315.
17. Osella, S.; Narita, A.; Schwab, M. G.; Hernandez, Y.; Feng, X.; Müllen, K.; Beljonne, D. Graphene nanoribbons as low band gap donor materials for organic photovoltaics: quantum chemical aided design. *ACS Nano* **2012**, *6*, 5539-5548.
18. Cheng, S. H.; Weng, T. M.; Lu, M. L.; Tan, W. C.; Chen, J. Y.; Chen, Y. F. All carbon-based photodetectors: an eminent integration of graphite quantum dots and two dimensional graphene. *Sci. Rep.* **2013**, *3*, 2694.
19. Wu, J.; Pisula, W.; Müllen, K. Graphenes as potential material for electronics. *Chem. Rev.* **2007**, *107*, 718-747.
20. Yan, X.; Cui, X.; Li, L.-S. Synthesis of large, stable colloidal graphene quantum dots with tunable size. *J. Am. Chem. Soc.* **2010**, *132*, 5944-5945.
21. Rieger, R.; Müllen, K. Forever young: polycyclic aromatic hydrocarbons as model cases for structural and optical studies. *J. Phys. Org. Chem.* **2010**, *23*, 315-325.

22. Tan, Y.-Z.; Yang, B.; Parvez, K.; Narita, A.; Osella, S.; Beljonne, D.; Feng, X.; Müllen, K. Atomically precise edge chlorination of nanographenes and its application in graphene nanoribbons. *Nat. Commun.* **2013**, *4*, 2646.
23. Narita, A.; Wang, X.-Y.; Feng, X.; Müllen, K. New advances in nanographene chemistry. *Chem. Soc. Rev.* **2015**, *44*, 6616-6643.
24. Wang, X.-Y.; Narita, A.; Müllen, K. Precision synthesis versus bulk-scale fabrication of graphenes. *Nat. Rev. Chem.* **2017**, *2*, 0100.
25. Paternò, G. M.; Nicoli, L.; Chen, Q.; Müllen, K.; Narita, A.; Lanzani, G.; Scotognella, F. Modulation of the nonlinear optical properties of dibenzo[hi,st]ovalene by peripheral substituents. *J. Phys. Chem. C* **2018**, *122*, 25007-25013.
26. Coles, D. M.; Chen, Q.; Flatten, L. C.; Smith, J. M.; Müllen, K.; Narita, A.; Lidzey, D. G. Strong exciton-photon coupling in a nanographene filled microcavity. *Nano Lett.* **2017**, *17*, 5521 – 5525.
27. Wang, X.; Zhi, L.; Tsao, N.; Tomović, Ž.; Li, J.; Müllen, K. Transparent carbon films as electrodes in organic solar cells. *Angew. Chem. Int. Ed.* **2008**, *47*, 2990-2992.
28. Abbas, A. N.; Liu, B.; Narita, A.; Dössel, L.; Yang, B.; Zhang, W.; Tang, J.; Wang, K. L.; Räder, H. J.; Feng, X. et al. Vapor-phase transport deposition, characterization, and applications of large nanographenes. *J. Am. Chem. Soc.* **2015**, *137*, 4453-4459.
29. Böhme, T.; Simpson, C. D.; Müllen, K.; Rabe, J. P. Current-voltage characteristics of a homologous series of polycyclic aromatic hydrocarbons. *Chem. –A Eur. J.* **2007**, *13*, 7349-7357.

30. Iyer, V. S.; Yoshimura, K.; Enkelmann, V.; Epsch, R.; Rabe, J. P.; Müllen, K. A soluble C 60 graphite segment. *Angew, Chem. Int. Ed.* **1998**, *37*, 2696-2699.
31. Paternò, G. M.; Chen, Q.; Wang, X. Y.; Liu, J.; Motti, S. G.; Petrozza, A.; Feng, X.; Lanzani, G.; Müllen, K.; Narita, A. et al. Synthesis of dibenzo[hi,st]ovalene and its amplified spontaneous emission in a polystyrene matrix. *Angew. Chem. Int. Ed.* **2017**, *56*, 6753-6757.
32. Dumsloff, T.; Yang, B.; Maghsoumi, A.; Velpula, G.; Mali, K. S.; Castiglioni, C.; De Feyter, S.; Tommasini, M.; Narita, A.; Feng, X. et al. Adding four extra k-regions to hexa-peri-hexabenzocoronene. *J. Am. Chem. Soc.* **2016**, *138*, 4726-4729.
33. Miseikis, V.; Convertino, D.; Mishra, N.; Gemmi, M.; Mashoff, T.; Heun, S.; Naghighian, N.; Bisio, F.; Canepa, M.; Piazza, V. et al. Rapid CVD growth of millimetre-sized single crystal graphene using a cold-wall reactor. *2D Mater.* **2015**, *2*, 014006.
34. Yin, Z.; Li, H.; Li, H.; Jiang, L.; Shi, Y.; Sun, Y.; Lu, G.; Zhang, Q.; Chen, X.; Zhang, H. Single-layer MoS₂ phototransistors. *ACS Nano* **2012**, *6*, 74-80.
35. Novoselov, K. S.; Geim A. K.; Morozov, S. V.; Jiang, D.; Zhang, Y.; Dubonos, S. V.; Grigorieva, I. V.; Firsov, A. A. Electric field effect in atomically thin carbon films. *Science* **2004**, *306*, 666-669.
36. Liu, X.; Luo, X.; Guo, H.; Wang, P.; Zhang, L.; Zhou, M.; Yang, Z.; Shi, Y.; Hu, W.; Ni, Z. et al. Epitaxial ultrathin organic crystals on graphene for high - efficiency phototransistors. *Adv. Mat.* **2016**, *28*, 5200–5205.

37. Chang, X.; Sun, Z.; Ho, K. Y.-F.; Tao, X.; Yan, F.; Kwok, W.-M.; Zheng, Z. A highly sensitive ultraviolet sensor based on a facile in situ solution-grown ZnO nanorod/graphene heterostructure. *Nanoscale* **2011**, *3*, 258.
38. Stokes, P.; Liu, L.; Zou, J.; Zhai, L.; Huo, Q.; Khondaker, S. I. Photoresponse in large area multiwalled carbon nanotube/polymer nanocomposite films. *Appl. Phys. Lett.* **2009**, *94*, 042110.
39. Yao, X.; Wang, X.-Y.; Simpson, C.; Paternò, G. M.; Guizzardi, M.; Wagner, M.; Cerullo, G.; Scotognella, F.; Watson, M. D.; Narita, A. et al. Regioselective hydrogenation of a 60-carbon nanographene molecule toward a circumbiphenyl core. *J. Am. Chem. Soc.* **2019**, *141*, 4230-4234.
40. Yu, Y.-J.; Zhao, Y.; Ruy, S.; Brus, L. E.; Kim, K. S.; Kim, P.; Tuning the graphene work function by electric field effect, *Nano Lett.* **2009**, *9*, 3430-3434.
41. Fantuzzi, P.; Martini, L.; Candini, A.; Corradini, V.; del Pennino, U.; Hu, X.; Feng, X.; Müllen, K.; Narita, A.; Affronte, M. Fabrication of three terminal devices by electrospray deposition of graphene nanoribbons. *Carbon* **2016**, *104*, 112-118.

Insert Table of Contents Graphic and Synopsis Here

